

1 **Intercomparison of in situ water vapor balloon-borne measurements from Pico-SDLA**  
2 **H<sub>2</sub>O and FLASH-B in the tropical UTLS**

3 M. Ghysels<sup>1</sup>, Riviere E.D.<sup>1</sup>, S. Khaykin<sup>2</sup>, C. Stoeffler<sup>1</sup>, N. Amarouche<sup>3</sup>, J.-P. Pommereau<sup>2</sup>, G.  
4 Held<sup>4</sup> and G. Durry<sup>1</sup>

- 5 1. Groupe de Spectrométrie Moléculaire et Atmosphérique, UMR CNRS 6089, UFR  
6 Sciences Exactes et Naturelles, Moulin de la Housse, BP 1039, 51687 Reims Cedex 2,  
7 France  
8 2. LATMOS, CNRS, Université de Versailles St Quentin, Guyancourt, Guyancourt, France.  
9 3. Division technique de l'Institut National des Sciences de l'Univers, 1, place Aristide  
10 Briand, 92195, Meudon Cedex, France.  
11 4. Instituto de Pesquisas Meteorológicas (IPMet)/ Universidade Estadual Paulista (UNESP),  
12 CX Postal, 281, 17015-970 Bauru, S.P., Brazil

13  
14 Correspondance email : M. Ghysels : melanie.ghysels@nist.gov

15  
16 **Abstract**

17 In this paper we compare water vapor mixing ratio measurements from two quasi-  
18 parallel flights of the Pico-SDLA H<sub>2</sub>O and FLASH-B hygrometers. The measurements were  
19 made on February 10, 2013 and March 13, 2012, respectively, in the tropics near Bauru, Sao  
20 Paulo St., Brazil during an intense convective period. Both flights were performed as part of a  
21 French scientific project, TRO-Pico, to study the impact of the deep-convection overshoot on  
22 the water budget. Only a few instruments that permit the frequent sounding of stratospheric  
23 water vapor can be flown within a small volume weather balloons. Technical difficulties  
24 preclude the accurate measurement of stratospheric water vapor with conventional *in situ*  
25 techniques. The instruments described here are simple and lightweight, which permits their  
26 low-cost deployment by non-specialists aboard a small weather balloon. We obtain mixing  
27 ratio retrievals which agree above the cold-point tropopause to within 1.9 % and 0.5 % for the  
28 first and second flights, respectively. This level of agreement for balloon-borne measured  
29 stratospheric water mixing ratio constitute one of the best agreement reported in the literature.  
30 Because both instruments show similar profiles within their combined uncertainties, we  
31 conclude that the Pico-SDLA H<sub>2</sub>O and FLASH-B datasets are mutually consistent.

32 **1. Introduction**

33 Water vapor in the stratosphere plays an important role in the radiative and chemical  
34 budget (Shindell et al, 1998, Herman et al, 2002, Loewenstein et al, 2002). Changes in the  
35 stratospheric humidity can have a significant impact on the climate and the radiative balance  
36 of the Earth atmosphere (Forster et al, 2002, Solomon et al, 2010, Riese et al, 2012). Climate  
37 models show that an increase in stratospheric humidity can lead to stratospheric cooling and  
38 consequently to a more important ozone depletion (Shindell, 2001, Dvorstov and Solomon,  
39 2001).

40 Regular radiosonde measurements are reliable only in the lower-to-middle troposphere  
41 zone, whereas high-precision hygrometers must be employed for stratospheric measurements  
42 because this region is so dry. Although, a variety of techniques have been developed for  
43 measuring water vapor in the stratosphere, achieving high accuracy measurements of  
44 humidity in the stratosphere is far from routine. Current stratospheric measurements of

45 humidity include: frost-point detection, light absorption using tunable diode laser  
46 spectrometers and fluorescence (Lyman- $\alpha$  radiation) methods. Usually, *in situ* instruments  
47 have a higher precision and a better spatial resolution than remote sensing instruments  
48 because the former measurements are performed directly inside the air mass and do not  
49 require geophysical inversion. Several balloon-borne measurements to monitor the  
50 stratospheric water vapor have been conducted since the early 1980's (Kley et al, 2000,  
51 Oltmans et al, 2000, Rosenlof et al, 2001, Vömel et al, 2002, Jensen et al, 2005, Read et al,  
52 2007, Vömel et al, 2007a, Vömel et al, 2007b, Jensen et al, 2008, Weinstock et al, 2009,  
53 Hurst et al, 2011, Berthet et al, 2013, Rollins et al, 2014, Kindel et al, 2015). In some cases,  
54 coincident flights have been realized leading to comparisons of *in situ* water vapor  
55 measurements (Jensen et al, 2005, Vömel et al, 2007a, Vömel et al, 2007b, Jensen et al, 2008,  
56 Weinstock et al, 2009, Hurst et al, 2011, Berthet et al, 2013). However, persistent  
57 disagreements remain. For example, (Vömel et al, 2007a), compared *in situ* balloon-borne  
58 measurements of water vapor from several instruments during coincident flights. Comparison  
59 of *in situ* water vapor measurements from the CFH hygrometer, the NOAA/CFD aircraft  
60 hygrometer and the Harvard Lyman- $\alpha$  hygrometer led to considerable discrepancies up to  
61 110%. Differences of  $\pm 10\%$  were found by comparing the FLASH-B and NOAA/CDML  
62 water vapor measurements obtained at altitudes of 15 km above the polar stratosphere (Vömel  
63 et al, 2007b). (Jensen et al, 2008) found that discrepancies between nearly simultaneous water  
64 vapor measurements in the TTL (Tropical Tropopause Layer) could reach 2 to 3 ppmv. More  
65 generally, in the TTL, the measurements have shown discrepancies larger than 10%. The  
66 main problem for *in situ* measurements of water vapor is contamination by outgassing from  
67 the balloon and the instrument structure. Recently, the proper selection of wall materials and  
68 the judicious positioning of the different elements have significantly reduced this confounding  
69 effect.

70 The TRO-Pico project, which is funded by the French National research Agency  
71 (ANR) for five years, was launched in 2010. The main objectives of TRO-Pico are to  
72 combine balloon-, ground-, and satellite-based observations as well as model simulations at  
73 different scales to study the impact of deep-convection overshoots on the stratospheric  
74 humidity. The balloon campaigns were realized during March 2012 and from November 2012  
75 to March 2013 in Bauru, Sao Paulo State, Brazil and were hosted by IPMet (Instituto de  
76 Pesquisas Meteorológicas). The campaigns were divided into two periods: the SMOP period  
77 (six-month observation period) to study the change of water vapor during the overall  
78 convective season and the IOP campaign (intensive observation period), occurring during the  
79 most intense convective period to study the troposphere-to-stratosphere transport and the  
80 stratospheric moistening impact. Both comparison flights discussed here are part of the IOP  
81 period. Within both periods, 31 successful water vapor flights were carried on under small  
82 zero-pressure balloons from 500 m<sup>3</sup> to 1500 m<sup>3</sup>, or 1.2 kg rubber balloons. Water vapor  
83 measurements were performed using two lightweight hygrometers: Pico-SDLA H<sub>2</sub>O and  
84 FLASH-B. A forthcoming paper will present the meteorological/dynamical analysis of the  
85 water vapor measurements linked to specific hydration in the lower stratosphere (S. M.  
86 Khaykin, personal communication, 2015).

87 In order to validate the observations, Pico-SDLA and FLASH were launched twice on  
88 the same day within a 3h interval close to the convection overshoot event: March 13, 2012

89 and February 10, 2013. These two cases will be discussed in this paper. These flights were  
90 performed using small weather balloons in order to limit the effect of water outgassing. Only  
91 a few instruments can be flown under such small volume balloons to permit regular  
92 soundings. Unlike other compact hygrometers where the speed-of-descent prevents accurate  
93 measurements, these instruments can measure stratospheric water vapor even during descent  
94 under parachutes.

95  
96 The purpose of this study is to thoroughly evaluate the accuracy of the water vapor  
97 measurements performed during this campaign and to quantify the consistency of the data  
98 produced by the two hygrometers. Both Pico-SDLA and FLASH hygrometers are described in  
99 the Sec. 2 and the flight train is described in Sec. 3. The *in situ* water vapor measurements in  
100 the TTL and lower stratosphere are compared for each of the flights in the Sec.4.

## 101 2. Instrumentation

### 102 2.1. The Pico-SDLA H<sub>2</sub>O hygrometer

103 Pico-SDLA H<sub>2</sub>O (hereafter Pico-SDLA) is a lightweight spectrometer which measures  
104 water vapor using laser absorption spectroscopy (Durry et al, 2008). The probe laser emits at a  
105 wavelength of 2.63  $\mu\text{m}$  and has a 1-m path length through ambient air. This hygrometer was  
106 flown during a coincident flight with the ELHYSA frost-point hygrometer in March 2011,  
107 leading to a stratospheric water vapor measurement comparison (Berthet et al, 2013). Both  
108 hygrometers agreed to within 3.5% in the polar stratosphere, which is well below their  
109 combined instrumental uncertainties.

110 The mass of the Pico-SDLA is less than 9 kg, making it suitable as a payload for small  
111 stratospheric balloons (500 and 1500 m<sup>3</sup>). Its design was improved in 2012 in order to meet  
112 the requirements of TRO-Pico campaigns. The electronic components are now integrated into  
113 a Rohacell box on the top of the cell, which makes the instrument more compact. Figure 1  
114 shows the new version of the hygrometer. It uses a distributed feedback (DFB) diode laser  
115 emitting at 2.63  $\mu\text{m}$ . The water vapor absorption line is scanned by tuning the laser current at  
116 fixed temperature. After passing through the ambient-air sample, the laser beam is focused  
117 onto an InAs detector using a sapphire lens. The mechanical structure of the sensor comprises  
118 carbon fiber tubes to strengthen the overall instrument, especially for the landing with  
119 parachutes. The instrument is equipped with a TM/TC antenna to transmit the spectrum data  
120 to the ground during the flight and to control instrument parameters in case intervention is  
121 required. The sensor is able to measure water vapor from the ground to altitudes of 35 km for  
122 concentrations ranging from 15000ppmv to less than 1 ppmv.

123 Two different rotation-vibration absorption transitions of water vapor are probed  
124 because of the large variation in mixing ratio occurring between the troposphere and the  
125 stratosphere. For measurements from the ground to around 200 hPa pressure level, we used  
126 the  $4_{13}\leftarrow 4_{14}$  H<sub>2</sub><sup>16</sup>O line at 3802.96561 cm<sup>-1</sup>. Above 200 hPa pressure level, we use the  
127  $2_{02}\leftarrow 1_{01}$  H<sub>2</sub><sup>16</sup>O line at 3801.41863 cm<sup>-1</sup>. During in-flight measurements, the switch from one  
128 line to the other is automatically driven. Both sets of line parameters are obtained from  
129 HITRAN 2012 database (Rothman et al, 2013). In HITRAN, the line intensities for these two  
130 lines is based on the work by R. A. Toth at JPL (Jet Propulsion Laboratory, NASA) with a

131 relative uncertainty of 2% (see “Linelist of water vapor parameters from 500 to 8000 cm<sup>-1</sup>” at  
132 <http://mark4sun.jpl.nasa.gov/h2o.html>). The water vapor transition is determined prior to the  
133 launch, thus allowing for automatic selection during in-flight measurements.

134 The mixing ratio is extracted from the measured spectra using a non-linear least  
135 squares fitting algorithm applied to the measured line shape. We use the Beer-Lambert law to  
136 model the spectrum and use a Voigt profile (VP) to describe the molecular line shape. We  
137 found that fitting the VP to the measured spectra yielded residuals consistent with the  
138 instrument noise. No evidence of systematic residuals caused by higher-order line shape  
139 effects were observed for stratospheric pressures (our region of interest). Figure 2 shows an  
140 example of three atmospheric spectra of the H<sub>2</sub>O 2<sub>02</sub>←1<sub>01</sub> line recorded during the February  
141 10, 2013 flight in Bauru, at different altitudes in the lower stratosphere (24.24 hPa ≡ 25.2 km;  
142 73.60 hPa ≡ 18.4 km; 101.05 hPa ≡ 16.6 km). During this flight, the cold point tropopause  
143 (hereafter CPT) altitude was approximately 16.7 km. In the upper panel, the black and red  
144 lines represent the measurement and fitted results, respectively. The corresponding fit  
145 residuals (meas.- fit) are shown in the bottom panel. The standard deviation of the residuals is  
146 around 2×10<sup>-4</sup> and corresponds to the noise level of the measured beam transmission. These  
147 residuals do not show any W structure which has been observed when the VP is fit to  
148 transitions exhibiting non-Voigt effects such as Dicke narrowing and/or speed-dependent  
149 effects (Dicke,1953, Rautian and Sobel’man, 1967, Tran et al, 2007, Boone et al,  
150 2007).Defining the spectrum signal-to-noise ratio (SNR) as the peak absorbance divided by  
151 the baseline standard deviation, we find a maximum SNR of approximately 65:1. For the  
152 relatively low pressures (20 hPa to 120 hPa) and hence low absorbances encountered in the  
153 TTL and in the lower stratosphere the VP provides an accurate representation of the measured  
154 spectrum for the noise levels of this spectrometer. At higher pressures (in the troposphere) a  
155 more sophisticated line shape may be necessary because the spectrum SNR may reveal  
156 systematic deviations from the VP.

157 Several tests were conducted to determine the sensitivity of the fitting procedure to the  
158 baseline interpolation, as well as to the temperature- and pressure-measurement uncertainties.  
159 These tests were realized using a synthetic spectrum with a noise level equivalent to the in-  
160 flight spectra. Details of these tests are given below.

161 The absorption spectrum is extracted from the atmospheric spectra by removing  
162 structure in the baseline which is induced by optical components and vibrations of the optical  
163 cell. The baseline is interpolated using a polynomial combined with a sinusoid term which  
164 takes into account commonly observed interference fringes caused by Fabry-Pérot effects  
165 between optics. The quality of the fitting procedure is influenced by the spectrum SNR, the  
166 polynomial order and the number of points chosen for the interpolation. The combined  
167 uncertainty introduced by these different factors varies with the peak absorbance of the line  
168 and consequently with the pressure level from 4.5 % at 50 hPa to 0.7 % at 150 hPa.

169 The air pressure is measured using a Honeywell absolute pressure sensor, which  
170 operates between -40°C and +85 °C with a manufacturer-specified relative uncertainty of  
171 0.05% full scale (0.7 hPa). The pressure measurements are corrected for drift caused by  
172 changes in temperature. During the TRO-Pico campaign flights, the atmospheric temperature  
173 ranged from -85 °C to +35 °C. In order to eliminate measurement error caused by being  
174 outside the instrument’s temperature operating range, the pressure sensor is placed inside an

175 enclosure having a minimum temperature of 0 °C. The uncertainty in the fitted water vapor  
176 concentration caused by temperature-dependent sensitivity of the pressure sensor temperature  
177 is estimated to be ~0.05%.

178 The temperature is measured using three SIPPICAN thermistors which are coated to  
179 limit solar radiation effects. These sensors are located on each end and at the center of the  
180 optical cell, providing an average temperature for the measurements. The rotation of the  
181 optical cell during the flight induces a temperature difference between the three thermistors,  
182 which varies from 0 to 5 °C. This depends on the solar exposure of the thermistors (in the case  
183 of daytime flights). For this reason, we select the lowest measured temperature for the data  
184 processing. Each sensor was calibrated independently by the manufacturer between -90 °C  
185 and +50 °C. The uncertainty of the temperature is specified to be 0.3 °C, yielding a 0.25 %  
186 uncertainty in the measured sample concentration.

187 By taking into account all sources of error that we can estimate (i.e spectroscopic and  
188 experimental errors, as well as error due to spectra processing), the combined relative  
189 standard uncertainty ranges from 7.5 % to 3.5 % in the TTL and the lower stratosphere,  
190 depending on the local conditions. Since temperature and pressure are input variables for the  
191 mixing ratio retrievals, we investigated the consistency of these measurements. We compared  
192 the Pico-SDLA measurements with those of a Vaisala RS-92 radiosonde during one  
193 coincident flight on January 18, 2013. Details of this work are provided in the next section.

#### 194 *2.1.1. Temperature and pressure measurements comparison on January 18, 2013*

195 On January 18, Pico-SDLA has been launched at 22:11 UTC under a 1500 m<sup>3</sup> balloon.  
196 The time is recorded in UTC using a GPS-disciplined clock located onboard the Pico-SDLA.  
197 One measurement is made every 300ms to 500 ms depending on the signal-to-noise ratio of  
198 the measurements and on the vertical speed of the payload during the flight. The  
199 measurements start as soon as they are requested by the operator, independently of launch  
200 time. The RS-92 radiosonde, attached to the same balloon, detects the launch time and records  
201 it as  $t=0$ . Thereafter, it takes one measurement every 10 seconds.

202 The data were synchronized by applying a small temporal offset to the time stamps.  
203 This offset was determined from the cross-correlation of the temperature profiles from both  
204 sensors and corresponded to the maximum of the cross-correlation.

205 We calculated the mean temperature difference (mean  $\Delta T$ ), the mean pressure  
206 difference (mean  $\Delta P$ ) as well as the standard deviations of the differences  $\sigma(\Delta T)$  and  $\sigma(\Delta P)$ .  
207 We only used the ascent measurements for the comparison. Although the descent of the Pico-  
208 SDLA occurs under parachute, this is not the case of the radiosonde which remains attached  
209 to the balloon. The vertical speeds of both sensors are consequently different therefore  
210 precluding correlation with time. Since only the descent measurements of Pico-SDLA are  
211 usable, the radiosonde is never attached to Pico-SDLA during this time. Indeed, the RS-92  
212 telemetry system at 403 MHz induces a modulation of the laser emission, which creates two  
213 sidebands on the spectrum rendering them unusable.

214 The temperature uncertainty on the RS-92 is 0.5 °C while the pressure uncertainty is  
215 quoted by the manufacturer for two pressure ranges : 1080hPa to 100 hPa and 100hPa to 3  
216 hPa, for which the combined standard uncertainty is 1.5 Pa, and 0.6 hPa, respectively.

217 The mean  $\Delta T$  for this flight is  $0.12^\circ\text{C}$  with a standard deviation  $\sigma(\Delta T)$  of  $0.28^\circ\text{C}$ .  
218 The mean  $\Delta T$  is less than both uncertainties. The  $\Delta T$  is always lower than  $0.5^\circ\text{C}$  except  
219 above 23 km where the RS-92 exhibited large spikes in the measured temperature. Therefore  
220 for this flight, we concluded that the RS temperature was unreliable above this altitude. The  
221 SIPPICAN and the RS-92 measurements agree well with the observations of (Nash et al,  
222 2010; Bower and Fitzgibbon, 2004) which were obtained by comparing different types of  
223 temperature sensors. In these studies, the comparison of temperature measurements, using  
224 corrected data, lead to temperature differences up to  $0.4^\circ\text{C}$  during night flights and  $1^\circ\text{C}$  for  
225 daytime flights. The differences are usually higher above the tropopause, which is probably  
226 due to icing of the sensor.

227 The mean pressure difference (mean  $\Delta P$ ) and the standard deviation of this difference  
228  $\sigma(\Delta P)$  are  $-0.024\text{hPa}$  and  $0.163\text{hPa}$  respectively. This pressure difference is below the  
229 uncertainties of both the Pico-SDLA and RS-92 pressure sensors. Between the ground and 2.6  
230 km, the pressure differences are as large as  $0.5\text{ hPa}$ . This behavior was also observed in the 8<sup>th</sup>  
231 WMO High Quality Radiosonde Intercomparison (Nash et al, 2010). During this campaign,  
232 the performance of radiosonde systems' pressure measurements was investigated. It was  
233 found that the pressure differences ranged from 0 to  $1.4\text{ hPa}$  and correlated with the altitude of  
234 the balloon. The biggest differences occurred near the ground.

235 We determined the consistency of measurement pairs using the GRUAN (Reference  
236 Upper-Air Network) analysis approach detailed by (Immler et al, 2010). Given two  
237 independent measurements  $m_1$  and  $m_2$  and their respective uncertainties  $u_1$  and  $u_2$ , these two  
238 measurements can be considered as consistent if:  $|m_1 - m_2| < k\sqrt{u_1^2 + u_2^2}$ . Here,  $k$  is the  
239 statistical significance factor. For  $k=1$  and if the condition is true, the measurements are  
240 consistent.

241 For measurements of temperature and taking into account each sensor uncertainty, we find  
242 that  $k\sqrt{u_1^2 + u_2^2} = 0.58$ . Thus, to be consistent, the measurements of absolute difference,  
243 expressed as  $|m_1 - m_2|$ , must be lower than 0.58. The mean temperature difference,  
244 calculated from in situ measurements, is  $0.05^\circ\text{C} \pm 0.15^\circ\text{C}$ . Likewise for pressure, the mean  
245  $\Delta P$  has to be less than  $0.92\text{ hPa}$ . In our case, the mean pressure difference is  $0.02\text{hPa} \pm 0.11$   
246  $\text{hPa}$ . For both parameters, the condition is satisfied and therefore, the measurements are  
247 consistent following the GRUAN approach.

### 248 2.1.2. Water vapor outgassing

249 Contamination of water vapor measurements caused by outgassing from the balloon  
250 envelope or instrument surfaces was first observed in the *in situ* measurements of  
251 (Mastenbrook, 1968) and (Zander, 1966). For the TRO-Pico campaign, the use of small-  
252 volume weather balloons ( $1500\text{ m}^3$  or  $500\text{ m}^3$ ) is expected to reduce the water vapor  
253 outgassing from the balloon envelope. We found that the ascent mixing ratio reached as high  
254 as 25 ppmv, whereas the mean stratospheric mixing ratio was 4 ppmv. Therefore, we used  
255 only the measurements obtained during descent. We compared these measurements from  
256 Pico-SDLA with those of FLASH-B to determine whether or not outgassing of water vapor  
257 contaminated the data. As described in detail in the following section, we found that the  
258 FLASH-B descent measurements did not suffer from outgassing contamination. During the

259 beginning of the descent, a small contamination (up to 0.5 ppmv and visible up to 3 km below  
260 the float altitude) of the Pico-SDLA data was observed. Therefore, we considered the Pico-  
261 SDLA data below the altitude where the contamination is observed.  
262

## 263 *2.2. The FLASH-B hygrometer*

264 The balloon version of FLASH is a compact lightweight sonde developed at the  
265 Central Aerological Observatory, Russia, for balloon-borne water vapour measurements in the  
266 upper troposphere and stratosphere (Yushkov et al, 1998). The instrument is based on the  
267 fluorescent method (Kley and Stone, 1978; Bertaux and Delannoy, 1978), which uses the  
268 photodissociation of H<sub>2</sub>O molecules exposed to vacuum ultraviolet radiation ( $\lambda < 137$  nm)  
269 followed by the measurement of the fluorescence of excited OH radicals using a Hamamatsu  
270 photomultiplier in photon-counting mode. The intensity of the fluorescent light sensed by the  
271 photomultiplier is directly proportional to the water vapor mixing ratio under stratospheric  
272 conditions (10–150 hPa). The H<sub>2</sub>O measurement range is limited to pressures lower than  
273 300hPa to 400 hPa because of strong Lyman-alpha absorption in the lower troposphere. The  
274 instrument uses an open optical layout, where the analyzed volume is located outside the  
275 instrument. This design allows reduction of the instrument size to that of a small sonde with a  
276 total mass(including batteries)of about 1 kg. This arrangement restricts the use of the  
277 instrument to night-time only.

278 Each FLASH-B instrument is calibrated in the laboratory against a reference dew-  
279 point hygrometer, MBW 373L. A description of the procedure can be found in (Vömel et al,  
280 2007b). The detection limit for a 4-s integration time at stratospheric conditions is  
281 approximately 0.1 ppmv, while the accuracy is limited by the calibration error amounting to a  
282 relative uncertainty of 4 %. The typical measurement precision in the stratosphere is 5 % to 6  
283 %, whereas the combined relative uncertainty in water vapor concentration is less than 10 %  
284 throughout the stratosphere. The FLASH-B has been successfully used in a number of balloon  
285 campaigns (e.g., LAUTLOS-WAVVAP, SCOUT-AMMA,TC4, LAPBIAT-II) which  
286 included simultaneous measurements of stratospheric water vapor by different measurement  
287 techniques. In particular, point-by-point comparison with the frost-point hygrometer from the  
288 NOAA CMDL showed a mean deviation of 2.4 % with 3.1 % standard deviation ( $1\sigma$ )  
289 (Vömel et al., 2007a), and comparison with CFH showed a mean deviation of 0.8 % with a 4  
290 % relative standard deviation (Khaykin et al., 2013).

291 The flight configuration of the FLASH-B, in which the analyzed volume is located  
292 beneath the downward-looking optics 2-3 cm away from the lens, caused noticeable self-  
293 contamination during balloon ascent because of water outgassing from the instrument surfaces  
294 and balloon. The contamination effect is observed as a quasi-exponential growth of water  
295 vapour readings above about 70 hPa during the ascent. This occurs because the relative  
296 contribution of water carried on the sounding equipment surfaces becomes more significant as  
297 the number density of ambient water molecules decreases with altitude. In contrast, the  
298 FLASH-B measurements during the descent at the bottom of the flight train in undisturbed air  
299 are free of contamination as shown by the reduction in water vapour readings immediately  
300 after the burst of balloon. Here we use the contamination-free descent profiles along with the  
301 clean ascent profiles below 75 hPa.

### 302 **3. Balloon Flight trains**

303 The flights have been realized under small zero pressure balloons of 500 m<sup>3</sup> and 1500  
304 m<sup>3</sup> volume for Pico-SDLA instruments and 1.2 kg rubber balloons for the FLASH  
305 instruments. The launch of these balloons was realized by the French scientific team, assisted  
306 by staff from IPMet.

307 During the SMOP period, regular soundings of the UT-LS using the Pico-SDLA H<sub>2</sub>O  
308 spectrometer were conducted by the technicians of IPMet without the presence of the French  
309 scientific teams. The hygrometer operation was simplified to permit its deployment by non-  
310 specialists. During this period, the hygrometer was deployed under 500 m<sup>3</sup> zero pressure  
311 Aerostar balloons.

312 For all flights, the flight train includes a parachute, a cutter device and a balloon  
313 telemetry/remote control system (E-track iridium), a strobe light and a radar reflector. The  
314 cutter device is used to separate the payload from the balloon, with the payload descending  
315 under the parachute. The E-Track iridium allows one to follow the flight train during the  
316 ascent and the descent and to initiate separation from the balloon. The scientific instrument is  
317 connected to the flight train by a nylon driss. The flight trains were easy to implement and  
318 permitted quick deployment of the instruments with respect to larger balloons.

319 For the water vapor flights of Pico-SDLA, the instrument was located at least 15 m  
320 below the balloon to limit outgassing from the balloon envelope. On March 13, 2012, the  
321 instruments of the flight train, from bottom to top, were the Pico-SDLA H<sub>2</sub>O, and the LOAC  
322 Optical Particle Counter. The total payload weight for this flight was 15 kg under a 500 m<sup>3</sup>  
323 balloon. On February 10, 2013, the instruments of the flight train, from bottom to top, were  
324 the Pico-SDLA H<sub>2</sub>O and the Pico-SDLA CH<sub>4</sub>. The total payload mass was 25 kg under a  
325 1500 m<sup>3</sup> balloon.

326 For flights of the FLASH-B, the E-Track box and cutter device were not included in  
327 the flight train. The instruments of the flight train were from bottom to top, the FLASH-B and  
328 the COBALD (Compact Optical Back-scatter Aerosol detector) backscatter sonde, on March  
329 13, 2012, and FLASH-B, COBALD and LOAC on February 11, 2013. The overall payload  
330 masses were 7.4 kg and 9.4 kg, respectively.

### 331 **4. Comparison of mixing ratio retrievals**

#### 332 ***4.1. Flight conditions***

333 The flights of February 10-11, 2013 and March 13, 2012 were intended to capture the  
334 signature of the overshoots in water vapor profiles. The launch site was located on the  
335 UNESP Bauru Campus, at the outskirts of town (Coordinates: 22.36 °S, 49.03 °W).

336 On February 10, 2013, the Pico-SDLA was launched at 21:03 UTC with overshooting  
337 conditions observed by the IPMet S-band radar located 200 km east of Bauru. Subsequently, a  
338 convective cell reached an altitude of >16 km, which was about 150 km east of the launch site  
339 position. On this day, the most intense convective events occurred between 18:06 and 21:15  
340 UTC. The FLASH-B hygrometer was launched at 0:09 UTC, 3 hours later than Pico-SDLA.

341 On March 13, 2012, Pico-SDLA H<sub>2</sub>O was launched at 19:20 UTC in convective  
342 conditions and FLASH-B was launched 3 hours later. On this day, strong convection was



343 observed until 21:00 UTC with convective cells reaching altitudes exceeding 18 km. Both  
344 instruments were able to catch the signature of an overshooting cell reaching 19.2 km.

345 During the descent, the vertical speed of the instruments ranged from 60 m/s (just after  
346 the flight train separates from the balloon) to 20 m/s in the TTL. In this condition, the Pico-  
347 SDLA spectra were recorded without any averaging or a maximum average of 5 spectra in  
348 order to achieve good vertical resolution and to avoid excessive overlapping of mixing ratio  
349 measurements from different layers of the TTL.

#### 350 **4.2. February 10-11, 2013**

351 Figure 3 shows the balloon trajectories of both instruments. On this plot we show the  
352 descent trajectory of Pico-SDLA and both the ascent and descent trajectory of FLASH-B  
353 wherever the ascent measurements of FLASH can be considered. The altitude of the  
354 trajectories is color coded. Altitudes between 14 km and 28 km are considered, representing  
355 the TTL and lower stratosphere, which are our regions of interest. For both instrument  
356 trajectories, the time is indicated in UTC. The ascent of Pico-SDLA lasted 1h41 min followed  
357 by a float of 7 min at 27.4 km before a 37-min-long descent. The ascent of FLASH-B lasted  
358 1h 31 min followed by a descent of 47 min. The maximum altitude reached by the balloon  
359 was 28.75 km. We can see in Fig. 3 that Pico-SDLA flew 25 km south of FLASH-B which  
360 resulted in some small differences in the observed water vapor enhancements.

361 In the case of Pico-SDLA, we use the water vapor measurements below 23 km  
362 because a small outgassing effect ( $\sim 0.4$  ppmv) is observed above this height. The balloon  
363 carrying the FLASH-B flight-train is much smaller than the 1500 m<sup>3</sup> balloon used for Pico-  
364 SDLA. Since such a small balloon limits water vapor outgassing, we can also consider the  
365 FLASH-B ascent profile up to approximately 18 km of altitude, above which a small  
366 outgassing effect starts to be observed. This leads to the comparison shown in Fig.4. In this  
367 figure, we compare *in situ* water vapor measurements between 15 km and 24.5 km from Pico-  
368 SDLA H<sub>2</sub>O and FLASH-B. The lower boundary of the TTL is defined in (Fueglistaler et al,  
369 2009) as the area above the level of the mean convective outflow ( $\sim 14$  km). The upper  
370 boundary is set at 70 hPa (18.8 km), above which the atmosphere is governed mainly by  
371 stratospheric processes. In Fig.4, the upper boundary of the TTL (green dot line) corresponds  
372 to an altitude of  $\sim 18.8$  km. The CPT of each instrument is determined from the descent  
373 temperature profiles and is shown by the orange and brown dashed lines. In the case of Pico-  
374 SDLA, the CPT is 16.63 km ( $-74.15$  °C) and for FLASH it is 16.98 km ( $-75.2$  °C). This  
375 altitude corresponds to the level of the minimum temperature and has an important role in the  
376 troposphere-to-stratosphere coupling and exchange. The water vapor transport from the  
377 troposphere to the stratosphere is partially dependent on the thermal characteristics of the CPT  
378 (Holton et al, 1995, Mote et al, 1996, Kim and Son, 2012, Randel and Jensen, 2013). Indeed,  
379 the coldest temperature encountered during the slow ascent partially determines the amount of  
380 dehydration of the air mass entering the stratosphere. The amount of water vapor and the  
381 temperature determine the relative humidity with respect to ice (RHi). At a given specific  
382 humidity, the coldest temperature will correspond to the highest RHi, thus the highest  
383 potential to nucleate ice particles that can fall, leading to a dehydration of the air entering the  
384 stratosphere. The altitude difference between the CPT altitudes from Pico-SDLA and FLASH  
385 can be attributed to three different factors : a natural temporal and spatial temperature

386 variability in the TTL, the measurements uncertainties and the temperature profile behavior in  
387 the TTL which complicates the determination of the CPT : for this flight and the March 13,  
388 2012 flight, the temperature profile in the TTL is quite constant with temperature variations of  
389 less than 0.3 °C, within the sensors uncertainties. Then the CPT altitude is determined using  
390 small structures in the profile.

391 Analyzing the profile comparison in more detail, we find that the main structures are  
392 well captured by both instruments above and around the CPT, although the amplitude of the  
393 local maxima/minima sometimes varies slightly. Three water vapor enhancement structures  
394 appear on the descent profile of Pico-SDLA at altitudes of 16.5 km, 17.2 km and 18 km. The  
395 structure at 16.5 km is captured by FLASH during the ascent but not during the descent and is  
396 shifted downwards by about 90 m in altitude compared to the Pico-SDLA. The amplitude of  
397 the enhancement is, in the case of FLASH, about 0.5 ppmv and around 0.68 ppmv for the  
398 Pico-SDLA. During the descent, the structure at 17.2 km was captured by FLASH-B at the  
399 same altitude and shifted up by 50 m. The descent profile of FLASH-B does not show any  
400 structure at this altitude. For both instruments, the amplitude of the enhancement is similar but  
401 the structure is slightly thicker in the case of FLASH (nominally 560 m) instead of 500 m for  
402 Pico-SDLA. The structure at 18 km was captured by FLASH-B at the ascent but not at the  
403 descent. Because of a small amount of outgassing, the profile above 17.7 km cannot be  
404 considered. Nevertheless, structures are visible. The small altitude difference is of the same  
405 order of magnitude as the GPS height uncertainty. It also must be considered that the  
406 hygrometers did not fly at exactly the same time.

407 Over the altitude range between 15 km and 23 km, comparison between the ascent of  
408 FLASH-B and the descent of Pico-SDLA leads to a mean difference of  $(0.13 \pm 0.33)$  ppmv. In  
409 the same altitude range, the comparison between the descent profiles of both instruments  
410 yields a mean mixing ratio difference of  $(0.08 \pm 0.39)$  ppmv. FLASH-B is dryer than Pico-  
411 SDLA by 0.08ppmv at the descent. Considering the 4.1 ppmv mean mixing ratio over the 15  
412 to 23 km altitude range, the differences observed correspond to 1.9 % (with a 1- $\sigma$  standard  
413 deviation of 9.5%). Restricting our comparison to above the CPT, the mean difference is then  
414  $(-0.13 \pm 0.15)$  ppmv (1- $\sigma$  standard deviation: 3.7 %). We clearly see the impact of the  
415 humidity variability in the lower TTL region on the statistical results. The strong humidity  
416 variability induces a larger standard deviation and therefore less precise results. Although  
417 both instruments were flown 3 hours apart, the measurements are in good agreement.

#### 418 ***4.3. March 13, 2012 flight***

419 Figure5 shows the trajectory plot for Pico-SDLA and FLASH flights on March 13,  
420 2012. As in Fig. 3, the altitude of the trajectories is color coded and the time is in UTC. Pico-  
421 SDLA flew 22 km to the west of FLASH. The ascent of Pico-SDLA lasted 1h49 min followed  
422 by a float of 14 min at 23.6 km before a 40-min-long descent. The ascent of FLASH-B lasted  
423 1h 15 min followed by a descent of 1h 12 min. The maximum altitude reached by FLASH  
424 was 21.6 km.

425 The comparison of water vapor mixing ratio profiles from FLASH and Pico-SDLA  
426 between 21.3 km and 15 km is shown in Fig.6. For this case, FLASH-B water vapor  
427 measurements are usable up to 21.3 km. Up to this altitude, Pico-SDLA measurements do not  
428 show any outgassing effects. In this figure, the CPT from Pico-SDLA (orange dashed line)

429 and FLASH (brown dashed line), are located at 17.95 km and 17.44 km respectively. The  
430 upper boundary of the TTL is shown with a green dotted line at 70 hPa pressure level,  
431 corresponding to an altitude of 18.6 km. The temperature profiles are also shown in orange  
432 and brown lines. The CPT is much colder in this case than for the February 10 flight (-79 °C  
433 in average instead of -74.6 °C).

434 The RS-92, integrated into FLASH, measures the geopotential altitude whereas the  
435 GPS onboard Pico-SDLA measures the geometric altitude, inducing a shift of 378 m in  
436 altitude. To correct for this difference, we used the altitude measurements from the COBALD  
437 backscatter sonde which are obtained from a GPS. Thus, we were able to reconstruct the  
438 FLASH altitude scale by interpolating the COBALD data with respect to the time into flight.  
439 In this case, a  $(188 \pm 7)$  m altitude difference is still observed between Pico-SDLA and  
440 FLASH water vapor mixing ratio profiles. Although the origin of the shift is not fully  
441 understood, one possible explanation is an initialization on FLASH or COBALD error at  
442 launch time. Because the Pico-SDLA and the E-track iridium GPS measurements agree to  $\pm$   
443 20 m between the CPT and 21.3 km, this excludes an error coming from Pico-SDLA GPS  
444 altitude measurements. In Fig. 6, a 188 m shift was applied to the FLASH profile. This shift  
445 was determined maximize the correlation coefficient between both profiles. We emphasize  
446 that the March 13, 2012 case was the only one where such a high difference in altitude was  
447 observed.

448 Applying the 188 m shift leads to a mean mixing ratio difference of  $(0.02 \pm 0.21)$   
449 ppmv between 15 km and 21.2 km between descent profiles. In this case, Pico-SDLA H<sub>2</sub>O is  
450 dryer by 0.02 ppmv. Considering the mean mixing ratio, around 4.3 ppmv, the relative  
451 difference represents  $\sim 0.5\%$  (with 1- $\sigma$  standard deviation of 4.6 %). This shows the excellent  
452 agreement between the FLASH and Pico-SDLA measurements, which were always within  
453 instrumental uncertainties despite the fact that both instruments were flown 3 h apart.

454 This profile comparison showed identical structures (at 17.4 km, 18.1 km and 18.7 km  
455 of altitude) and mostly with a similar amplitude. Also, the altitude ranges of these structures  
456 are very close. The local maximum at 18.1 km (Fig. 6) stands out with a mixing ratio of 4.09  
457 ppmv in both Pico-SDLA and FLASH measurements. The structure is a little bit thicker for  
458 Pico-SDLA (300 m) than for FLASH (200 m). Also, besides the maximum value being  
459 identical for both instruments, the amplitude of the water vapor enhancement is slightly  
460 higher for Pico-SDLA (about 0.8 ppmv) whereas FLASH-B shows a 0.65 ppmv enhancement.  
461 An airmass trajectory analysis by (S. M. Khaykin, personal communication, 2015) shows that  
462 this enhancement is caused by a hydration from overshooting convection, which is about 65  
463 km away from the balloons. The differences in the amplitude of the signal by both  
464 instruments can easily be explained by the difference of time of the flights with respect to  
465 very local/short duration process. As a result, the instruments cannot sample the same process  
466 amplitude. Figure 5 shows the trajectory of both balloons, highlighting the relatively close  
467 trajectories which are slightly shifted in space. This helps account for the slight differences  
468 between the two profiles. Investigating another large water vapor enhancement at 18.7 km,  
469 both instruments measure the same local maximum of 4.19 ppmv. Both the vertical amplitude  
470 of the signal (500 m) and the amplitude of the enhancement based on the difference between  
471 the bottom of this layer and the local maximum is very similar  $\sim 1$  ppmv. (S. M. Khaykin,  
472 personal communication, 2015) shows that this enhancement is due to large scale mid-latitude

473 air intrusion, bringing higher mixing ratios of water into the tropical regions. However it  
474 should be noted that the shape of this enhancement is sharper for Pico-SDLA than for  
475 FLASH-B. No significant patterns are highlighted above this layer (~19 km) and both  
476 instruments report very similar mixing ratios.

## 477 **5. Pico-SDLA/FLASH-B correlation**

478 Figure 7 shows a scatter plot comparison of Pico-SDLA versus FLASH water vapor  
479 measurements for the flights of March 13, 2012 and February 10, 2013. The data are color  
480 coded by pressure in the altitude range from the CPT altitude up to the altitude free of out-  
481 gassing for each flight. A linear fit of the Pico-SDLA versus FLASH data is shown as a solid  
482 line.

483 We have calculated the Pearson's  $r$  coefficient from 15 km and from the CPT altitude.  
484 This coefficient is calculated from the linear least-squares fitting of the scatter plot data and  
485 represents the correlation coefficient.

486 For the February 10, 2013 flight results,  $r=0.92$  for the 15 km to 23 km range and  
487  $r=0.95$  for the CPT (16.7 km to 23 km) range. In this case, the water vapor enhancements at  
488 17.2 km and 18 km, which are seen by Pico-SDLA but not by FLASH as well as the humidity  
489 variability in the lower TTL region, have a significant impact on the correlation.

490 In the case of the March 13, 2012 flights, the correlation coefficient is mainly affected  
491 by the two large water vapor enhancements observed at 18.1 km and 18.7 km and which do  
492 not have exactly the same thickness and amplitude. Within 15 km to 21.2 km, the  $r$  is equal to  
493 0.98. Surprisingly,  $r$  decreases to 0.89 between the CPT (17.7 km) and 21.2 km. The  
494 statistical weight of the two structures at 18.1 km and 18.7 km is larger in the calculation  
495 when only altitudes above CPT are considered.

496 Because the two sensors did not fly at the same time, the correlation is strongly  
497 affected by the variability in the water vapor enhancement structures shown by the two  
498 different hygrometers. This effect is clearly visible through the changes in  $r$  between the two  
499 altitude ranges. In the case of March 13, 2012  $r$  is strongly affected by the two enhancement  
500 structures (one is even present above the TTL upper limit). Despite the evident impact of the  
501 vertical structures on the results, the present comparison exhibits some of the best agreement  
502 found in the literature for studies realized from coincident flights (Weinstock et al, 2009;  
503 Khaykin et al, 2013). In each case, the water vapor enhancements are of much larger  
504 amplitude than the difference between the two instruments. FLASH and Pico-SDLA are  
505 therefore able to see, with good accuracy, the impact of dynamical process on water vapor  
506 concentrations.

## 507 **6. Summary and conclusions**

508 This work compares *in situ* water vapor measurements from two hygrometers: Pico-  
509 SDLA H<sub>2</sub>O and FLASH-B, obtained during the TRO-Pico balloon campaign held in Brazil  
510 between 2012 and 2013. It serves as the basis for a future paper (S. M. Khaykin, personal  
511 communication, 2015), centered on the meteorological analysis of the measurements.

512 The hygrometers were deployed on March 13, 2012 and February 10, 2013 when an  
513 overshooting convection event was observed in the vicinity of the flight paths. The impact of

514 overshoots on water vapor mixing ratios is visible on March 13, 2012, by the presence of  
515 three vertical structures at 17.4 km, 18.1 km and 18.7 km. A detailed analysis of this profile  
516 will be given in the forthcoming paper (S. M. Khaykin, personal communication, 2015).

517 The water vapor profiles were compared within two altitude ranges : above 15 km and  
518 above the CPT. The comparison above 15 km shows larger deviations (up to 9.5 %) than  
519 those above the CPT (around 4%) because of humidity variability in the uppermost  
520 troposphere. On March 13, 2012 and February 10, 2013, the mean difference of mixing ratios  
521 is 0.5 % and 1.9 %, respectively, above the CPT altitude; differences which are well below  
522 both instrument uncertainties. The differences are then much lower than the amplitude of the  
523 water vapor enhancements (between 0.5 ppmv and 0.8 ppmv) permitting us to reliably detect  
524 these overshoot signatures. Because the hygrometers were not flown at the same time, the  
525 humidity variability through the TTL had an important impact on the correlation coefficient  
526 and on the mixing ratio differences between the two instruments. Nevertheless, the  
527 differences observed in this study are well below the majority of *in situ* comparisons in the  
528 TTL and constitute one of the best intercomparison results by comparison to the work of  
529 (Weinstock et al, 2009; Khaykin et al, 2013). In these previous studies, the mixing ratio  
530 differences for *in situ* measurements ranged between 0.8 % and 5% and were obtained for  
531 coincident flights. In the context where persistently large disagreements exist between *in situ*  
532 measurements, the present work shows that Pico-SDLA H<sub>2</sub>O and FLASH-B are suitable for  
533 accurate *in situ* water vapor measurements over a variety of conditions, such as those  
534 including strong convection and high vertical speed. Furthermore, given the small differences  
535 observed among the profiles of each instrument, it can be concluded that the H<sub>2</sub>O data  
536 provided by the TRO-Pico campaign made of Pico-SDLA and FLASH-B measurements are  
537 mutually consistent. The compactness of these instruments permits their deployment under  
538 small weather balloons and therefore allows frequent soundings of the upper troposphere and  
539 lower stratosphere to be performed.

## 540 **Acknowledgements**

541 This work and the TRO-Pico project were supported by Agence Nationale de la  
542 Recherche (ANR) under Contract ANR-2010-BLAN-609-01 and by the region Champagne-  
543 Ardenne in France. The authors are grateful for the logistical and infrastructural support  
544 provided by IPMet/UNESP under a collaborative agreement with the French CNRS. We also  
545 thank IPMet's technicians, Hermes França, Bruno Biazon and Demilson Quintão for their  
546 assistance during the TRO-Pico campaigns and the Dr. Joseph T. Hodges from NIST for his  
547 greatly appreciated help reviewing this paper.

548

## 549 **References:**

(Bertaux and Delannoy, 1978) Bertaux, J. L. and Delannoy, A. : Premières mesures  
stratosphériques par un hygromètre à fluorescence ultra-violette, C. R. Acad. Sci. Paris, 286,  
191-194, 1978.

(Berthet et al, 2013) Berthet, G., Renard, J.-B., Ghysels, M., Durry, G., Gaubicher, B., and  
Amarouche, N. : Balloon-borne observations of mid-latitude stratospheric water vapour at two

launching sites: comparisons with HALOE and MLS satellite data, *J. Atmos. Chem.*, 70, 197-219, 2013

(Boone et al, 2007) Boone, C., D., Walker, K., A. and Bernath, P., F. : Speed-dependent Voigt profile for water vapor lines in infrared remote sensing applications, *J. Quant., Spectrosc. Ra.*, 105, 525-532, 2007.

(Bower and Fitzgibbon, 2004) Bower, C., A. and Fitzgibbon, J., J. : National Weather Service In-situ Radiation Temperature Correction for Radiosonde Replacement System GPS Radiosondes, Eighth Symposium on Integrated Observing and Assimilation Systems for Atmosphere, Oceans, and Land Surface, Seattle, USA, January 10, 2004.(Chaboureau et al, 2007) Chaboureau, J.,-P., Cammas, J.,-P., Duron, J.,Mascart, P., J., Sitnikov, N., M., and Voessing, H.,-J. :A numerical study of tropical cross-tropopause transport by convective overshoots, *Atmos. Chem. Phys.*, 7, 1731-1740, 2007

(Chemel et al, 2009) Chemel, C., Russo,M.,R.,Pyle, J., A.,Sokhi, R., S., and Schiller, C. : Quantifying the Imprint of a Severe Hector Thunderstorm during ACTIVE/SCOUT-O3 onto the Water Content in the Upper Troposphere/Lower Stratosphere, *Mon. Wea. Rev.*, 137, 2493–2514, 2009, doi: <http://dx.doi.org/10.1175/2008MWR2666.1>

(Dauhut et al, 2015) Dauhut, T., Chaboureau, J.-P., Escobar, J. and Mascart, P. :Large-eddy simulations of Hector the convective making the stratosphere wetter. *Atmosph.Sci. Lett.*, 16, 135–140. doi: 10.1002/asl2.534, 2015

(Dicke , 1953) Dicke, R., H. : The effect of collisions upon the Doppler width of spectral lines, *Phys. Rev.*, 89, 472-473, 1953

(Dvorstovand Solomon, 2001) Dvorstov, V.,L.,andSolomon, S. :Response of the stratospheric temperatures and ozone to past and future increases in stratospheric humidity, *J. geophys. Res.*, 106, 7505-7514, (2001)

(Durry et al, 2008) Durry, G., Amarouche, N., Joly, L., Liu, X.,Parvitte, B., and Zeninari, V. : Laser diode spectroscopy of H<sub>2</sub>O at 2.63  $\mu$ m for atmospheric applications, *Appl. Phys. B* 90, 573-580, 2008

(Forster et al, 2002) Forster, P., M., F. and Shine, K.,P. :Assessing the climate impact of trends in stratospheric water vapor, *Geophys. Res. Lett.*, 29, issue 6, 10-1 -10-4, 2002

(Fueglistaler et al, 2005) Fueglistaler, S., Bonazzola, M., Haynes, P., H., and Peter, T. : Stratospheric water vapor predicted from the Lagrangian temperature history of air entering the stratosphere in the tropics, *J. Geophys. Res.*, 110 (D8), doi:10.1029/2004JD005516, 2005.

(Fueglistaler et al, 2009) Fueglistaler, S., Dessler, A., Dunkerton, T., Folkins, I., Fu,Q.,andMote, P., W. : Tropical tropopause layer, *Rev. Geophys.*, 47, 1, 2009

(Grosvenor et al, 2007) Grosvenor,D., P.,Choularton, T., W.,Coe,H., and Held, G. : A study of the effect of overshooting deep convection on the water content of the TTL and lower stratosphere from Cloud Resolving Model simulations, *Atmos. Chem. Phys.*, 7, 4977–5002, 2007

(Herman et al, 2002) Herman, R., L.,Drdla, K., Spackman, J., R., Hurst, D., F., Popp, P., J., Webster, C., R.,Romashkin, P., A., Elkins, J., W., Weinstock, E., M.,Gandrud, B., W.,Toon, G., C.,Schoeberl,M., R.,Jost, H., Atlas, E., L. and Bui, T., P. :Hydratation, dehydration, and the total hydrogen budget of the 1999/2000 winter Arctic stratosphere, *J. Geophys.Res.*, 107, 2002-2014, 2002

(Holton et al, 1995) Holton, J. R., Haynes, P. H., McIntyre, M. E., Douglass, A. R., Rood, R. B., and Pfister, L. :Stratosphere-troposphere exchange. *Rev. Geophys.*, 33, 403–439, 1995

(Hurst et al, 2011) Hurst,D., F.,Hall,E., G.,Jordan,A., F.,Miloshevich,L., M.,Whiteman,D.,N.,Leblanc, T.,Walsh,D.,Vömel,H.,andOltmans,S.,J. : Comparisons of temperature, pressure and humidity measurements by balloon-borne radiosondes and frost point hygrometers duringMOHAVE-2009, *Atmos. Meas. Tech.*, 4, 2777-2793, 2011

(Immler et al, 2010) Immler, F., J., Dykema, J., Gardiner,T., Whiteman, D., N., Thorne,P., W. and Vömel,H. : Reference Quality Upper-Air Measurements: guidance for developing GRUAN data products, *Atmos. Meas. Tech.*, 3, 1217–1231, 2010

(James et al, 2008) James, R., M. Bonazzola, B.,Legras, K., Surbled, and Fueglistaler, S. : Water vapor transport and dehydration above convective outflow during Asian monsoon, *Geophys. Res. Lett.*, 35, L20810, doi:10.1029/2008GL035441, 2008.

(Jensen et al, 2005) Jensen E., J., Smith, J., B., Pfister, L., Pittman, J., V., Weinstock, E., M., Sayres, D., S., Herman, R., L., Troy, R., F., Rosenlof, K., Thompson, T., L., Fridlind, A., M., Hudson, P., K., Cziczo, D., J., Heymsfield, A., J., Schmitt, C., and Wilson, J. C. : Ice supersaturations exceeding 100% at the cold tropical tropopause: implications for cirrus formation and dehydration, *Atmos. Chem. Phys.*, 5, 851-862, 2005.

(Jensen et al, 2008) Jensen, E. J., Pfister, L., Bui, T., V., Lawson, P., Baker, B., Mo, Q., Baumgardner, D., Weinstock, E., M., Smith, J., B., Moyer, E., J., Hanisco, T., F., Sayres, D., S., Clair, J., M. St., Alexander, M., J., Toon, O., B., and Smith, J., A. : Formation of large (~ 100  $\mu\text{m}$ ) ice crystals near the tropical tropopause, *Atmos. Chem. Phys.*, 8, 1621–1633, doi:10.5194/acp-8-1621-2008, 2008.

(Khaykin et al, 2009) Khaykin, S., Pommereau, J.-P., Korshuno, L., Yushkov, V., Nielsen, J., Larsen, N., Christensen, T., Garnier, A., Lukyanov, A., and Williams, E. : Hydration of the lower stratosphere by ice crystal geysers over land convective systems, *Atmos. Chem. Phys.*, 9, 2275-2287, 2009.

(Khaykin et al, 2013) Khaykin, S. M., Engel, I., Vömel, H., Formanyuk, I. M., Kivi, R., Korshunov, L. I., Krämer, M., Lykov, A. D., Meier, S., Naebert, T., Pitts, M. C., Santee, M. L., Spelten, N., Wienhold, F. G., Yushkov, V. A., and Peter, T.: Arctic stratospheric dehydration – Part 1: Unprecedented observation of vertical redistribution of water, *Atmos. Chem. Phys.*, 13, 11503-11517, doi:10.5194/acp-13-11503-2013, 2013.

(Kim and Son, 2012) Kim, J. and Son, S.-W., *J. Climate*, 25, 5343-5360, 2012.

(Kindel et al, 2015) Kindel, B., C., Pilewskie, P., Schmidt, K., S., Thornberry, T., Rollins,A.,andBui, T. :Upper-troposphere and lower-stratosphere water vapor retrievals from the 1400 and 1900 nm water vapor bands, *Atmos. Meas. Tech.*, 8, 1147–1156, 2015

(Kley and Stone, 1978) Kley, D. and Stone, E. J. :Measurements of water vapor in the stratosphere by photodissociation with Ly  $\alpha$  (1216 Å) light, *Rev. Sci. Instrum.*, 49, 691-697, 1978.

(Kley et al, 2000) Kley, D., Russell III, J., M., and Phillips, C. :SPARC assessment of upper tropospheric and stratospheric water vapour, World Meteorol. Org., Geneva, 2000.

(Liu et al, 2010) Liu, X. M., Rivière, E. D., Marécal, V., Durré, G., Hamdouni, A., Arteta, J., and Khaykin, S. : Water vapor budget associated to overshoots in the tropical stratosphere: mesoscale modelling study of August 4-5, 2006 during SCOUT-AMMA, *Atmos. Chem. Phys.*, 10, 8267-8286, 2010.

(Loewenstein et al, 2002) Loewenstein, M., Jost, H., Grose, J., Eilers, J., Lynch, D., Jensen, S., and Marmie, J.: Argus : a new instrument for the measurement of the stratospheric dynamical tracers, N<sub>2</sub>O and CH<sub>4</sub>, *Spectrochim. Acta, Part A, Mol. Biomol. Spectrosc.*, 58, 2329-2347, 2002

(Mastenbrook, 1968) Mastenbrook, H., J. : Water vapor distribution in the stratosphere and High troposphere, *J. Atmos. Sci.*, 25, 299-311, 1968

(Mahesh et al, 1997) Mahesh, A., Walden, Von, P., and Warren, G. : Radiosonde temperature measurements in strong inversions : correction for thermal lag based on an experiment at the South Pole, *J. Atmos. Ocean. Tech.*, 14, 45-53, 1997.

(Miloshevich et al, 2004) Miloshevich, L., M., Paukkunen, A., Vömel, H., and Oltmans, S., J. : Development and validation of a time-lag correction for Vaisala radiosonde humidity measurements, *J. Atmos. Ocean. Tech.*, 21, 1305-1327, 2004.

(Mote et al, 1996) Mote, P., W., Rosenlof, K. H., McIntyre, M., E., Carr, E., S., Gille, J., C., Holton, J., R., Kinnersley, J., S., Pumphrey, H., C, Russell III, J., M., Waters, J., W. : An atmospheric tape recorder : the imprint of tropical tropopause temperatures on stratospheric water vapor, *J. Geophys. Res.*, 3989-4006, 1996.

(Nash et al, 2006) Nash, J., Smout, R., Oakley, T., Pathack, B., Kurnosenko, S. : WMO Intercomparison of high quality radiosonde systems, final report, February 2005.

(Nash et al, 2010) Nash, J., Oakley, T., Vömel, H., Wei, L., I. : WMO intercomparison of high quality radiosonde systems, Instruments and observing methods report No. 107, 2011

(Oltmans et al, 2000) Oltmans, S., J., Vömel, H., Hofmann, D., J., Rosenlof, K., H. and Kley, D. : The increase in stratospheric water vapor from balloonborne, frostpoint hygrometer measurements at Washington, D.C., and Boulder, Colorado, *Geophys. Res. Lett.*, 27, 3453-3456, 2000

(Randel and Jensen, 2013) Randel, W., J. and Jensen, E., J. : Physical processes in the tropical tropopause layer and their roles in a changing climate, *Nat. Geosci.*, 6, 196-176, 2013.

(Rautian and Sobel'man, 1967) Rautian, S., G., and Sobel'man, I., I. : The effect of collisions on the Doppler broadening of spectral lines, *Sov. Phys. Uspekhi*, 9, 701-716, 1967.

(Read et al, 2007) Read, W., G., Lambert, A., Bacmeister, J., Cofield, R., E., Christensen, L., E., Cuddy, D., T., Daffer, W., H., Drouin, B., J., Fetzer, E., Froidevaux, L., Fuller, R., Herman, R., Jarnot, R., F., Jiang, J., H., Jiang, Y., B., Kelly, K., Knosp, B., W., Kovalenko, L., J., Livesey, N., J., Liu, H.-C., Manney, G., L., Pickett, H., M., Pumphrey, H., C., Rosenlof, K. H., Sabouchi, X., Santee, M., L., Schwartz, M., J., Snyder, W., V., Stek, P., C., Su, H., Takacs, L., L., Thurstans, R., P., Vömel, H., Wagner, P., A., Waters, J., W., Webster, C., R., Weinstock, E., M., and Wu, D., L. : Aura Microwave Limb Sounder upper tropospheric and lower stratospheric H<sub>2</sub>O and relative humidity with respect to ice validation, *J. Geophys. Res.*, 112, 2007, D24S35, doi:10.1029/2007JD008752.

(Riese et al, 2012) Riese, M., Ploeger, F., Rap, A., Vogel, B., Konopka, P., Dameris, M. Forster, P. Impact of uncertainties in atmospheric mixing on simulated UTLS composition and related radiative effects *Journal of Geophysical Research-atmospheres*, 2012, 117, D16305

(Rollins et al, 2014) Rollins, A., W., Thornberry, T., D., Gao, R., S., Smith, J., B., Sayres, D., S., Sargent, M., R., Schiller, C., Krämer, M., Spelten, N., Hurst, D., F., Jordan, A., F., Hall, E., G., Vömel, H., Diskin, G., S., Podolske, J., R., Christensen, L., E., Rosenlof, K., H., Jensen, E.,



J., and Fahey, D., W. : Evaluation of UT/LS hygrometer accuracy by intercomparison during the NASA MACPEX mission, *J. Geophys. Res. Atmos.*, 119, 1915-1935, doi:10.1002/2013JD020817, 2014

(Rosenlof et al, 2001) Rosenlof, K., H., Oltmans, S., J., Kley, D., Russel III, J., M., Chiou, E., W., Chu, W., P., Johnson, D., G., Kelly, K., K., Michelsen, H., A., Nedoluha, G., E., Remsberg, E., E., Toon, G., C. and McCormick, M., P. : Stratospheric water vapor increases over the past half-century, *Geophys. Res. Lett.*, 28, 1195-1198, 2001

(Rothman et al, 2013) Rothman, L., S., Gordon, I., E., Babikov, Y., Barbe, A., Chris Benner, D., Bernath, P., F., Birk, M., Bizzocchi, L., Boudon, V., Brown, L., R., Campargue, A., Chance, K., Cohen, E., A., Coudert, L., H., Devi, V., M., Drouin, B., J., Fayt, A., Flaud, J., -M., Gamache, R., R., Harrison, J., J., Hartmann, J., -M., Hill, C., Hodges, J., T., Jacquemart, D., Jolly, A., Lamouroux, J., Le Roy, R., J., Li, G., Long, D., A., Lyulin, O., M., Mackie, C., J., Massie, S., T., Mikhailenko, S., Müller, H., S., P., Naumenko, O., V., Nikitin, A., V., Orphal, J., Perevalov, V., Perrin, A., Polovtseva, E., R., Richard, C., Smith, M., A., H., Starikova, E., Sung, K., Tashkun, S., Tennyson, J., Toon, G., C., Tyuterev, V., G., and Wagner, G. : The HITRAN 2012 molecular spectroscopic database, *JQSRT*, 130, 4-50, (2013)

(Shoeberl et al, 2011) Schoeberl, M. R. and Dessler, A. E.: Dehydration of the stratosphere, *Atmos. Chem. Phys.*, 11, 8433-8446, doi:10.5194/acp-11-8433-2011, 2011.

(Shoeberl et al, 2013) Schoeberl, M. R., Dessler, A. E., and Wang, T.: Modeling upper tropospheric and lower stratospheric water vapor anomalies, *Atmos. Chem. Phys.*, 13, 7783-7793, doi:10.5194/acp-13-7783-2013, 2013.

(Shindell et al, 1998) Shindell, D., T., Rind, D., and Lonergan, P. : Increased polar stratospheric ozone losses and delayed eventual recovery owing to increasing greenhouse-gas concentrations, *Nature*, 392, 589-592, 1998

(Shindell, 2001) Shindell, D., J. : Climate and ozone response to increased stratospheric water vapor, *Geophys. Res. Lett.*, 28, 1551-1554, 2001

(Solomon et al, 2010) Solomon, S., Rosenlof, K., H., Portmann, R., W., Daniel, J., S., Davis, S., M., Sanford, T., J., and Plattner, G., -K. : Contributions of stratospheric water vapor to decadal changes in the rate of global warming, *Science*, 327 (5970), 1219-1223, 2010

(Tran et al, 2007) Tran, H., Bermejo, D., Domenech, J., -L., Joubert, P., Gamache, R., R. and Hartmann, J. -M. : Collisional parameters of H<sub>2</sub>O lines : Velocity effects on the line-shape, *J. Quant., Spectrosc. Ra.*, 108, 126-145, 2007.

(Vömel et al, 2002) Vömel, H., Oltmans, S., J., Johnson, B., J., Shiotani, M., Fujiwara, M., Nishi, N., Agama, M., Cornejo, J., Paredes, F., and Enriquez, H. : Balloon-borne observations of water vapor and ozone tropical upper troposphere and lower stratosphere, *J. Geophys. Res.*, 107, NO. D14, doi: 10.1029/2001JD000707, 2002

(Vömel et al, 2007a) Vömel, H., David, D., E., and Smith, K. : Accuracy of tropospheric and stratospheric water vapor measurements by the cryogenic frost point hygrometer : Instrumental details and observations, *J. Geophys. Res.*, 112, Issue D8, 2007

(Vömel et al, 2007b) Vömel, H., Yushkov, V., Khaykin, V., Korshunov, V., Kyrö, E., Kivi, R. : Intercomparisons of stratospheric water vapor sensors : FLASH-B and NOAA/CMDL frost-point hygrometer, *J. Atmos. Ocea. Tech.*, 24, 941-952, doi: 10.1175/JTECH2007.1, 2007

(Weinstock et al, 2009) Weinstock, E., M., Smith, J., B., Sayres, D., S., Pittman, J., V., Spackman, J., R., Hints, E., J., Hanisco, T., F., Moyer, E., J., St. Clair, J., M.,

Sargent, M. R., and Anderson, J. G. : Validation of the Harvard Lyman- $\alpha$  in situ water vapor instrument : implications for the mechanisms that control stratospheric water vapor, *J. Geophys. Res.*, 114, D23301, doi:10.1029/2009JD012427, 2009

(Yushkov et al, 1998) Yushkov, V. Astakhov V., and Merkulov, S. : Optical balloon hygrometer for upper-troposphere and stratosphere water vapor measurements, in : *Proceedings SPIE 3501, Optical Remote Sensing of the Atmosphere and Clouds Beijing, China, September 14, 1998*, 439–445, 1998

(Zander et al, 1966) Zander, R. : Moisture contamination at altitude by balloon and associate equipment, *J. Geophys. Res.*, 71, 3775-3778, 1966.

Figure captions :

Fig. 1: Description of the Pico-SDLA H<sub>2</sub>O hygrometer, improved for the TRO-Pico campaign (2012-2013).

Fig. 2: Atmospheric spectra of the  $2_{02}\leftarrow 1_{01}$  line of H<sub>2</sub><sup>16</sup>O from Pico-SDLA H<sub>2</sub>O measurements on February, 10, 2013 during the descent of the flight. The top panel shows three experimental spectra (black line) and the results from fitting procedure (red line). These spectra were recorded at 25.2 km (24.24 mbar), 18.4 km (73.6 mbar) and 16.5 km (101.05 mbar) of altitude. The bottom panel shows the fit residuals for each spectrum.

Fig. 3: Balloon trajectories of Pico-SDLA and FLASH flights on February 10 and February 11, 2013. The trajectories are color coded with altitude. The time is given in UTC. The ascent and descent time stamps correspond to time when balloon was passing an altitude of 14 km.

Fig. 4: Comparison of water vapor *in situ* measurements from Pico-SDLA H<sub>2</sub>O and FLASH-B hygrometers in the TTL and lower stratosphere for the flight of February 10, 2013. The descent water vapor vertical profile of Pico-SDLA is represented by the solid black line. The ascent and descent water vapor profiles from FLASH-B are shown as solid blue and red lines respectively. The temperature profiles from Pico-SDLA and FLASH are shown in orange and brown lines. The CPT altitude is given by the orange and brown dashed lines for Pico-SDLA and FLASH respectively. The upper boundary of the TTL is shown is given by the green dotted line.

Fig. 5: Balloon trajectories of Pico-SDLA and FLASH flights on March 13, 2012. The trajectories are color coded with altitude. The time is given in UTC. The ascent and descent time stamps correspond to the time when the balloon passed an altitude of 14 km.

Fig. 6: Comparison of water vapor *in situ* measurements from Pico-SDLA H<sub>2</sub>O and FLASH-B hygrometers in the TTL and lower stratosphere for the flight of March 13, 2012. The descent water vapor vertical profile of Pico-SDLA is represented by a solid black line. The ascent and descent water vapor profiles from FLASH-B are shown in solid blue and red lines respectively. The temperature profiles from Pico-SDLA and FLASH are shown in solid orange and brown lines. The CPT altitude is given by the orange and brown dashed lines for Pico-SDLA and FLASH respectively. The upper boundary of the TTL is shown by the green dotted line.

Fig. 7 : Scatter plot comparison of Pico-SDLA versus FLASH water vapor measurements between the CPT and the free-of-outgassing altitude (21.3 km on March 13, 2012 and 23 km on February 10, 2013). The linear fit of the data is represented with solid blue and black lines for the March 13, 2012 and February 10, 2013 flights respectively. The data are color mapped by the pressure.

Figure 1



Figure 2

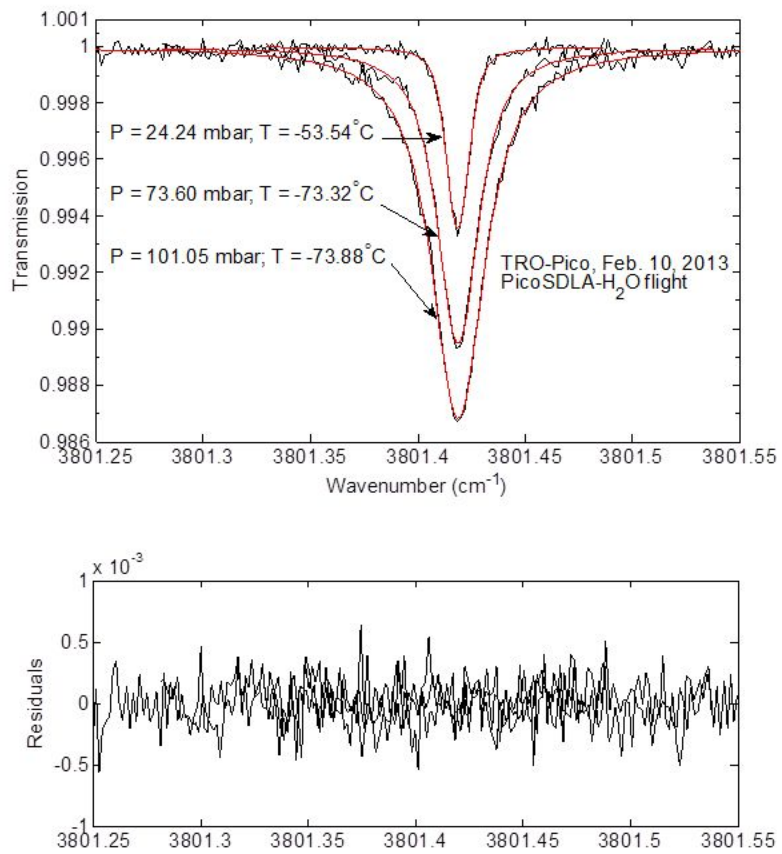


Figure 3

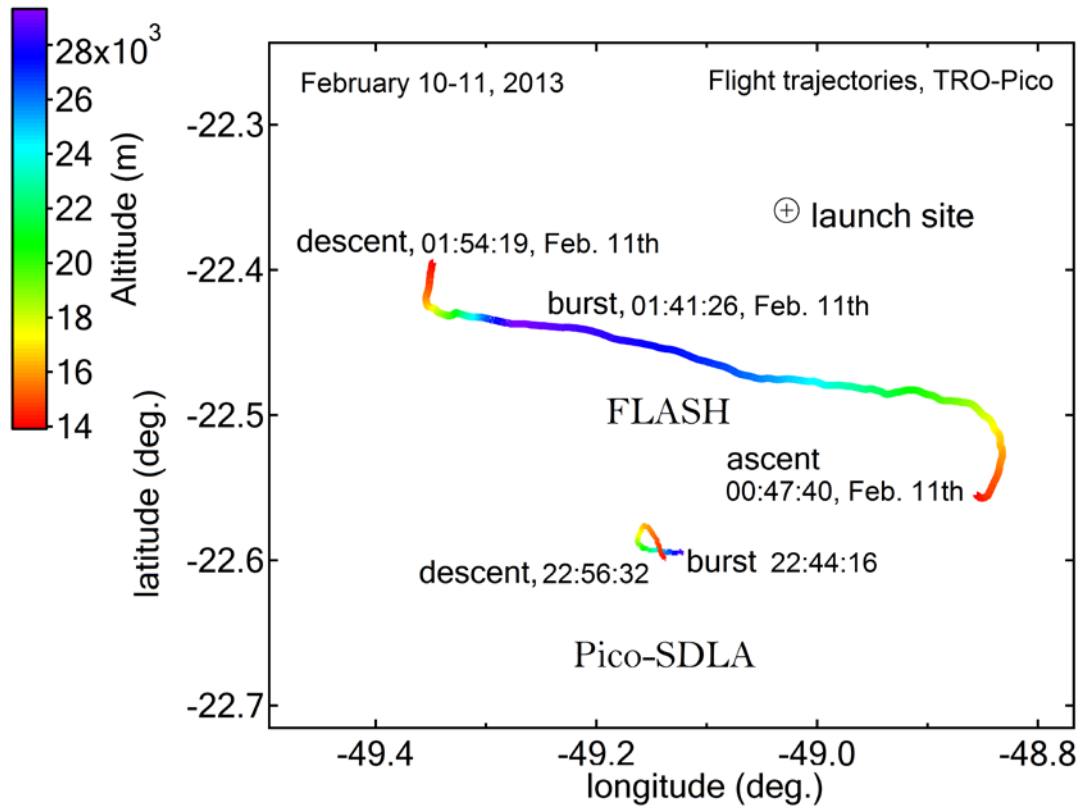


Figure 4

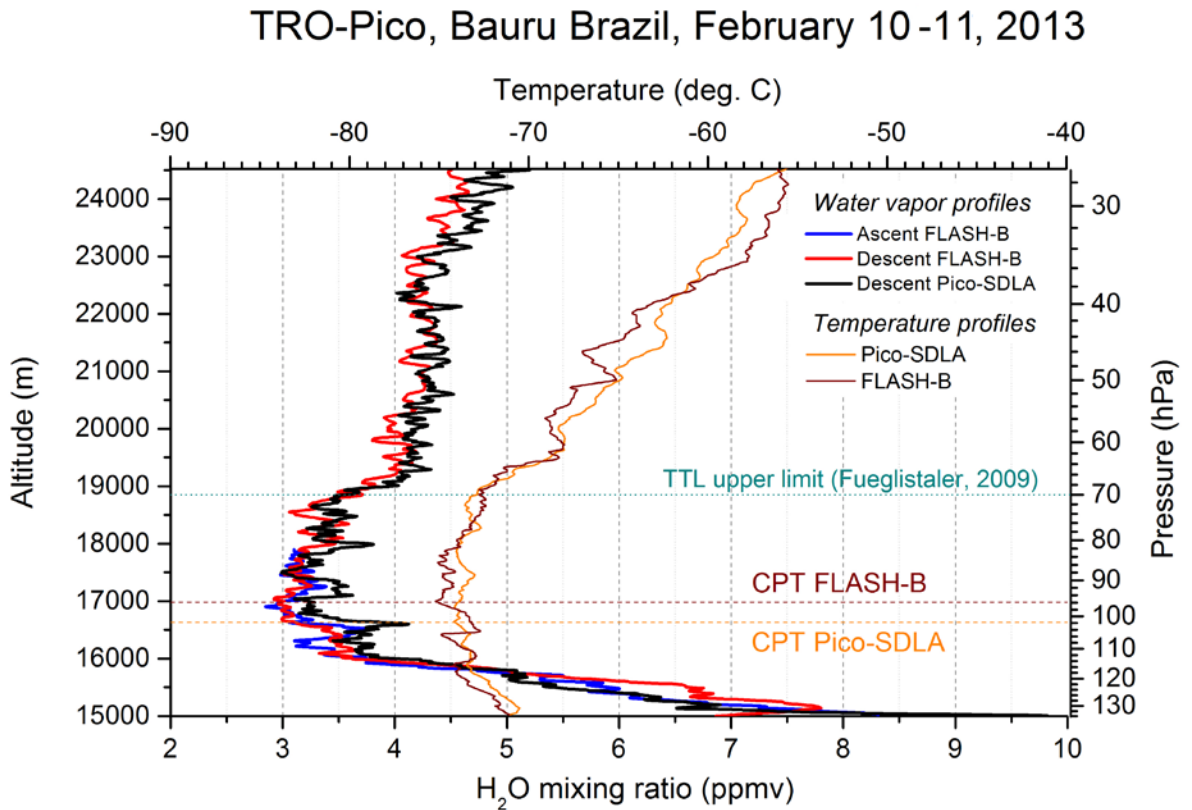


Figure 5

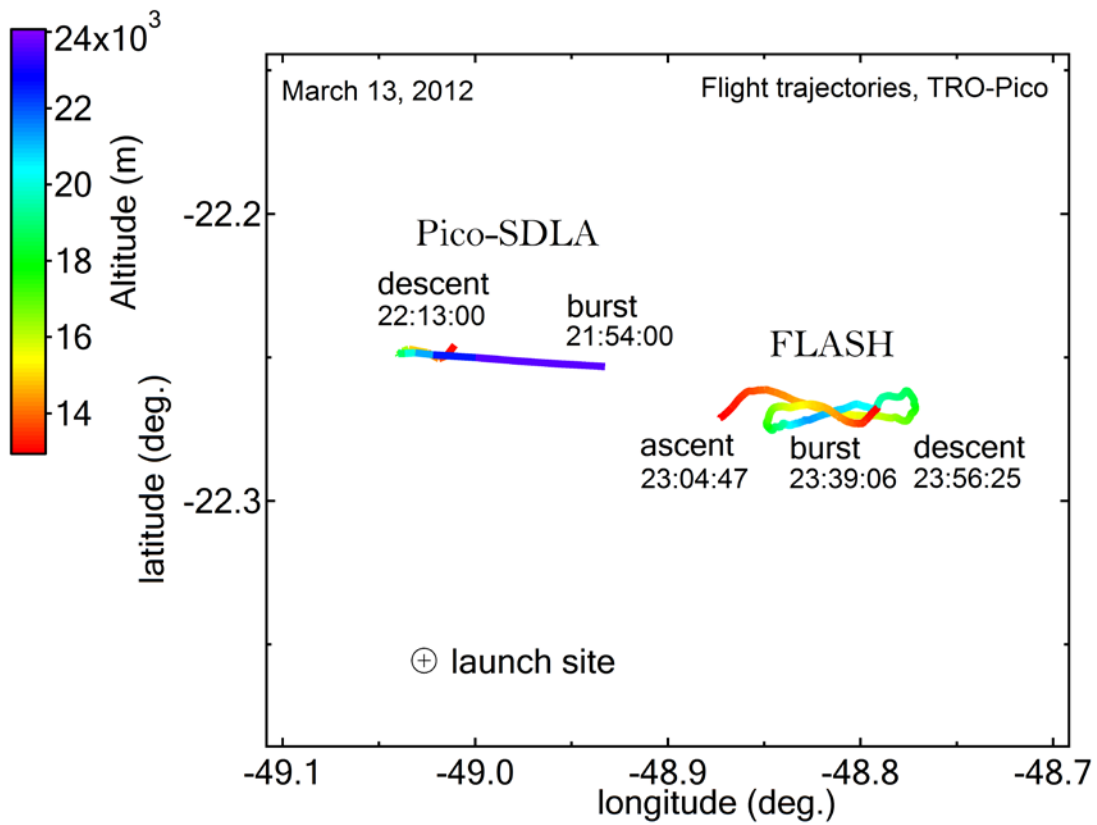


Figure 6

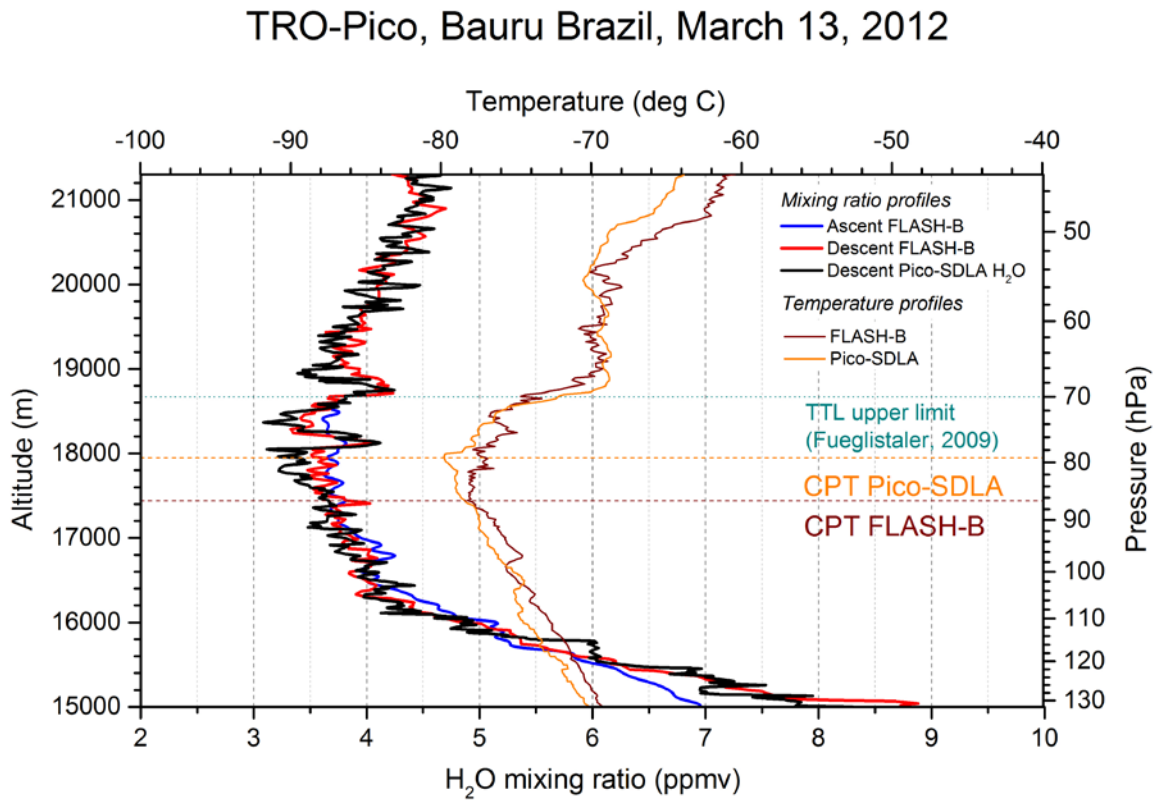


Figure 7

